RESEARCH ACTIVITIES III
Department of Electronic Structure

III-A States of Molecular Associates in Solutions

States of molecular association particularly in aqueous solutions are of great importance in understanding the role of molecules in living organism. Our recent studies of low frequency Raman spectroscopy of binary aqueous solutions of alcohols and carboxylic acids have shown that these amphiphilic molecules form microphases of clusters with the same solute species. This observation is in accord with the results of the ultrasonic absorption measurement of the binary mixtures. Kaatze and his coworkers found that acetic acid/water mixtures shows two relaxation terms attributed to the existence of two microphases, one with high and the other with low water contents. The water rich phase was assumed to fill the space between the acid-rich microphase aggregates. They also reported that the fluctuation correlation lengths in monohydric alcohol/water mixtures were expected to exceed some molecular diameters in contrast to much longer lengths expected for acid-rich phases in carboxylic acid/water mixtures. Low frequency Raman spectroscopy provides information on local structure of solutions coupled with hindered translational and librational motions. The Raman signals originating from dipole-induced dipole interaction are dominated with the interaction between the neighboring molecules. Theoretical prediction of intermolecular vibrational frequencies and Raman intensities is also applied for the assignment of observed Raman bands. These results are discussed not only with the mass spectrometric measurement of the clusters isolated from the liquid droplets through adiabatic expansion in vacuum, but also with the X-ray diffraction studies.

III-A-1 Raman Spectroscopic Study on Acetic Acid Clusters in Aqueous Solutions: Dominance of Acetic-Acid Association Producing Micro-Phases

NISHI, Nobuyuki; NAKABAYASHI, Takakazu; KOSUGI, Kentaroh[1]
(*[1]GUAS*)

With the addition of water into liquid acetic acid, the C=O stretching vibration band of acetic acid shows high frequency shift from 1665 cm^{-1} to 1715 cm^{-1}. This means that the hydrogen-bond of the C=O group of acetic acid is not so strong as those seen in liquid acetic acid or in CCl$_4$ solution (in which the band appears at 1668 cm^{-1}). A bent type hydrogen-bond is accountable for this observation. On the other hand, the increase of acetic acid in water drastically decreases the intensity of the hydrogen-bonded O-H stretching Raman band of water at 3200 cm^{-1}. This suggests that acetic acid breaks the hydrogen-bond networks of water. Low frequency $R(\bar{v})$ spectra of acetic acid/water binary solutions are reexamined with new experimental data and ab initio molecular orbital analysis of intermolecular vibrational modes. The $R(\bar{v})$ spectrum of the aqueous mixture at $x_A = 0.5$ bears a very close resemblance to that of the acetic acid/methanol mixture with $x_A = 0.5$, indicating that the molecular complexes responsible to the Raman spectra are acetic acid clusters. The calculated low-frequency Raman feature of a side-on type dimer with bent-type hydrogen-bonds based on ab initio molecular orbital theory reproduces the observed Raman pattern nicely. Any evidence of the formation of stable acid-water pairs is not found in the low frequency Raman spectra. Furthermore, an isosbestic point is seen in the region of $0.1 \leq x_A$ (mole fraction of acetic acid) ≤ 0.5, and another one is also observed in $0.5 \leq x_A \leq 1.0$. The observed spectra in the region of $0 < x_A < 0.5$ are reproduced simply by linear combinations of the pure water spectrum and the spectrum at $x_A = 0.5$. Figure 1 shows some examples of the spectral analyses. These results strongly suggest the presence of the two microphases with homogeneously associated molecules: a water cluster phase and an acetic acid cluster phase. The spectral change in $0.5 < x_A < 1.0$ is attributed to the coexistence of the acetic acid cluster phase in aqueous environment and the acid associated phase characteristic of liquid acetic acid.
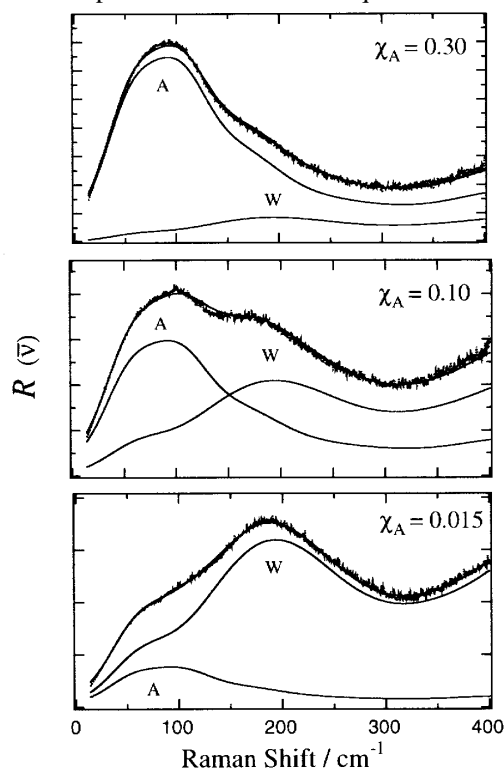
Figure 1. Decomposition of the observed $R(\bar{v})$ spectra of the binary solutions with $x_A = 0.015$, 0.10 and 0.30 into linear combination of the $R(\bar{v})$ spectra of pure water and the mixture with $x_A = 0.5$. The sum spectra calculated by a least square fitting are shown with solid lines.

III-A-2 Structures and Energies of Acetic Acid Aggregates in Aqueous Solution Studied by the RISM-SCF Method

NAKABAYASHI, Takakazu; SATO, Hirofumi; NISHI, Nobuyuki; HIRATA, Fumio

Acetic acid has been thought to form a cyclic dimer having a planar ring structure of C_{2h} symmetry in aqueous solution. From an analysis of Raman spectra of acetic acid/water binary solutions, however, we have suggested that a side-on dimer, not the cyclic dimer, is most likely for acetic acid in aqueous solution (structures of both the dimers are depicted in Figure 1). This means that the side-on dimer is more stable than the cyclic dimer in aqueous solution, although the cyclic structure is quite stable in the gas phase. In the present study, we calculate the hydrogen-bonding energies and structures of the cyclic dimer and the side-on dimer in aqueous solution by the RISM-SCF method. The advantage of the RISM-SCF method is to maintain the molecular aspects of solvents and thus to appropriately describe local interactions such as hydrogen bonds. The total energies and their energy components calculated for the monomer and the dimer species are collected in Table 1. The total energy (E_{tot}) in the RISM-SCF theory is defined as the sum of the following three energy components: (1) the electronic energy of solute molecule in the gas phase (E_{iso}), (2) the reorganization energy arising from the relaxation of the electronic

structure and the molecular geometry upon transferring solute from gas to aqueous solution (E_{reorg}), and (3) the excess chemical potential coming from solute-solvent interaction ($\Delta\mu$). The RISM-SCF calculations predict that the excess chemical potential of the side-on dimer is lower by 7.0 kcal/mol than that of the cyclic dimer. From the decomposition of the excess chemical potential into its constituents, the contribution from one of the carbonyl-oxygen atoms, which is free from the hydrogen bonding interaction with the other acetic acid molecule, is found to be much greater than the other atoms. Owing to such a stabilization in the side-on dimer, the energy difference between the two clusters is calculated to be reduced in solution; 2.0 kcal/mol in solution compared with 8.1 kcal/mol in the gas phase. Since the dipole moment of the side-on dimer is estimated to be 4.0 Debye in contrast to the null dipole moment of the cyclic dimer, the dipole-dipole interaction between the side-on dimers is expected to be sufficiently large. It is thus conceivable that the interaction energy between the side-on dimers exceeds over that between the cyclic dimers and contributes the stability of the side-on dimers in aqueous solution.
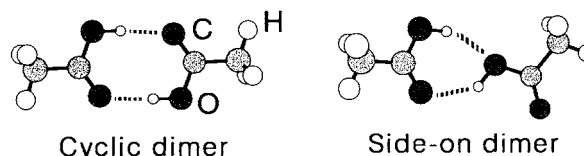
Figure 1. Structures of acetic acid dimers.

Table 1. Total energies and their energy components of acetic acid monomer and dimers in aqueous solution at the HF/DZP level.

	E_{total} (hartress)	E_{gas} (hartless)	E_{reorg} (kcal/mol)	$\Delta\mu$ (kcal/mol)
cis-Monomer	-227.8648503	-227.8721748	3.94	0.66
Cyclic dimer	-455.7318117	-455.7672506	4.05	18.19
Side-on dimer	-455.7270251	-455.7543088	5.96	11.16

III-A-3 Rayleigh Wing Spectra and Microphase Formation

NISHI, Nobuyuki; NAKABAYASHI, Takakazu; KOSUGI, Kentaroh[1]
([1]GUAS)

Motion of molecular clusters causing dipole-dipole or dipole-induced dipole interaction between the clusters can be observed in a very low frequency Raman spectrum of a solution. Rousset *et al.*[1] assumed that the low frequency temperature-dependent Raman scattering comes from oscillations of transient water aggregates with a somewhat ordered structure on the basis of the Raman studies of nuclei in glasses and silica particles in aerogels. Orientational relaxation coupled with long range dipole-dipole interaction can be also responsible to the Raman spectrum at the low frequency of 1–20 cm^{-1}. Figure 1 shows Bose-Einstein (BE) corrected very low frequency Raman spectra of water (spectrum A), aqueous mixtures with $x_A = 0.0075$ (spectrum B) and

0.07 (spectrum C). As reported by Rousset *et al.*,[1] the water spectrum at 298 K exhibits a hump at 10 cm^{-1}. This signal is temperature dependent in intensity and the position. The frequency increases with increasing temperature and falls to zero at –30 °C. Addition of a small amount of acetic acid in water enhances the wing intensity drastically, particularly in the region from 4 to 8 cm^{-1}. The 10 cm^{-1} component in the water spectrum in the figure must be related to this orientational relaxation of large water clusters. Rousset *et al.* estimated the average size of the clusters at room temperature to be 11 Å. In the aqueous mixture of acetic acid, orientational relaxation of the clusters is expected to take much longer time than that of water because of their longer sizes and larger dipole moments of the side-on type acetic acid dimer and higher clusters with this dimer unit. The clusterization of acetic acid molecules with large dipole-dipole interaction thus provides us a reasonable elucidation for the enhanced activity of the very low frequency Raman component as compared with that of water. The microphase model is in accord

with the present observation of the enhancement in the very low frequency component of the Raman spectra of the mixtures. As expected from the crystal structure of acetic acid, dipole-dipole interaction could be dominated in the acetic acid clusters elongating the lifetimes of the clusters in aqueous solutions.
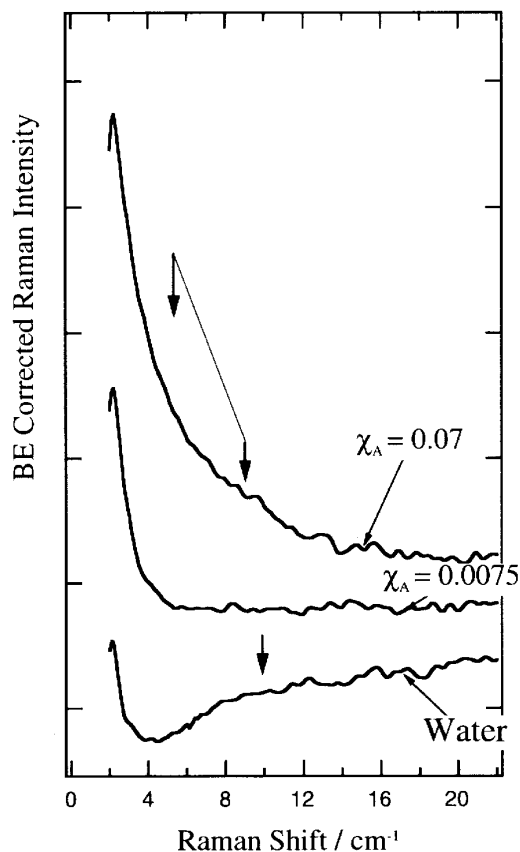
Figure 1. Mixing ratio dependence of the $R(\bar{v})$ spectra in acetic acid-water binary system.

III-A-4 Structures of Clusters in Methanol-Water Binary Solutions Studied by Mass Spectrometry and X-ray Diffraction

TAKAMUKU, Toshiyuki[1]; YAMAGUCHI, Toshio[2]; ASATO, Masaki[3]; MATSUMOTO, Masaki[3]; NISHI, Nobuyuki
([1]Saga Univ.; [2]Fukuoka Univ.; [3]Kyushu Univ.)

The structure of clusters in methanol-water binary solutions has been investigated as a function of methanol mole fraction, x_M, by mass spectrometry on clusters isolated from submicron droplets by adiabatic expansion in vacuum and by X-ray diffraction on the bulk binary solutions. The mass spectra have shown that the average hydration number, $<n_m>$, for m-mer methanol clusters, $M_m W_n$ (M = methanol, and W = water), decreases with increasing mole fraction of methanol, accompanied with two inflection points approximately at $x_M = 0.3$ and 0.7. Figure 1 shows the plots of average hydration numbers, $<n_m>$, for methanol m-mer hydrates with $m = 6$, 8, 10 and 12. The X-ray diffraction data have also revealed a similar change in

the number of hydrogen bonds per water and/or methanol oxygen atom at 2.8 Å to that found from mass spectrometry. On the basis of the results from the two methods, the most likely models of clusters formed in the binary solutions have been proposed; at $0 \leq x_M \leq 0.3$ the tetrahedral-like water clusters are the main species, at $0.3 \leq x_M \leq 0.7$ chain clusters of methanol molecules are gradually evolved with increasing methanol content, and at $x_M \geq 0.7$ chain clusters of methanol molecules become predominant. A comparison of the present results on the methanol-water mixtures with those of ethanol-water ones has shown that the tetrahedral-like water structure is broken down at a lower mole fraction of 0.2 and more sharply in the ethanol-water mixtures than in the methanol-water ones due to the large hydrophobic effect of ethanol. The behavior of the heat of mixing with varying alcohol concentration in the methanol-water mixtures is consistent with that of the average clusters formed in the mixtures, and thus anomalies in the physico-chemical data of alcohol-water probably originate from clusters formed in the mixtures.
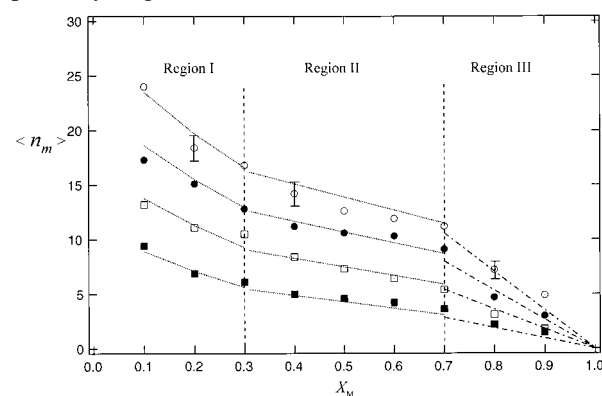
Figure 1. Plots of average hydration numbers, $<n_m>$, for methanol m-mer hydrates with $m = 6$ (■), 8 (□), 10 (●) and 12 (○) as functions of methanol mole fractions (x_m). Dotted lines were obtained from the equations: $<n_m> = 3(m - 0.5)(x_M - 0.3)^2 + 0.45(m - 3.8)$ for $0 \leq x_M \leq 0.3$, $<n_m> = m (x_M - 0.3)^2 + 1.4(m - 3.8)$ for $0.3 \leq x_M \leq 0.7$, and $<n_m> = 4.3(m - 3.8)x_M$ for $x_M \geq 0.7$.

III-A-5 Structure and Dynamics of 1,4-Dioxane-Water Binary Solutions Studied by X-ray diffraction, Mass Spectrometry, and NMR Relaxation

TAKAMUKU, Toshiyuki[1]; YAMAGUCHI, Atsushi[1]; TABATA, Masaaki[1]; NISHI, Nobuyuki; YOSHIDA, Koji[2]; WAKITA, Hisanobu[2]; YAMAGUCHI, Toshio[2]
([1]Saga Univ.; [2]Fukuoka Univ.)

The structure of clusters formed in 1,4-dioxane-water binary solutions has been investigated at ambient temperature as a function of 1,4-dioxane concentration by X-ray diffraction for the corresponding solutions and by mass spectrometry for liquid droplets formed in vacuum from the liquid mixtures by an adiabatic expansion method. The ^2H spin-lattice relaxation times of D_2O and 1,4-dioxane-d_8 molecules in 1,4-dioxane-water binary solutions have also been measured at 30 °C

over a whole range of 1,4-dioxane mole fraction. It has been found from the analysis of X-ray radial distribution functions that the number of hydrogen-bonds per water and 1,4-dioxane oxygen atom decreases with increasing 1,4-dioxane mole fraction X_{dio}, accompanied by two inflection points at approximately $X_{dio} = 0.1$ and 0.3: at $X_{dio} \geq 0.3$ the inherent structure of 1,4-dioxane is mostly observed, water molecules probably involved in the structure by hydrogen bonding, and at $0.15 \leq X_{dio} \leq 0.2$ both structures of water and 1,4-dioxane are ruptured to form small binary clusters of one or two dioxane and several water molecules. The mass spectra have revealed that at $X_{dio} = 0.01$ water clusters W_n (W = water) are mostly formed, but with increasing X_{dio} to 0.4 the water cluster reduced with evolving 1,4-dioxane clusters D_mW_n (D = 1,4-dioxane). The ^2H spin-lattice relaxation data of D_2O molecules in the mixtures showed that the rotation of water molecules is gradually retarded with increasing X_{dio} to 0.3, where the rotation is the slowest, and is then gradually accelerated with further increase in X_{dio}. The corresponding data of 1,4-dioxane-d_8 molecules showed a similar tendency, but the slowest motion observed at $X_{dio} = 0.2$. The present microscopic cluster structure and dynamic properties of the mixtures are discussed in connection with the heat of mixing, viscosity, and hydrophobic hydration.

III-B Ultrafast Dynamics of Photoexcited Molecules Studied by Transient Absorption and Transient Raman Spectroscopy Methods

Ultrafast transient absorption spectroscopy and transient Raman spectroscopy is now an universal and popular method for the study of reaction pathways induced by electronic or vibrational excitation of organic or metal complex molecules. We have constructed a new femto-pico synchronized multi-laser beam system. This unique system is open for collaborations in the field of molecular science.

III-B-1 Construction of a Tunable and Synchronized Picosecond-Femtosecond Double Laser System for the Study of Photodissociation Dynamics of Molecular Clusters in Solution

NAKABAYASHI, Takakazu; SATO, Shin-ichiro; INOKUCHI, Yoshiya; WATANABE, Kazuo; SAKAI, Makoto; FUJII, Masaaki; NISHI, Nobuyuki

Many time-resolved spectroscopic techniques require two broadly and independently tunable, synchronized light pulses with sufficient pulse energies. Since femtosecond time resolution simultaneously implies the loss of frequency resolution, a complementary use of picosecond and femtosecond pulse lasers is attractive for studying molecular dynamics. In order to meet these requirements, we have first constructed a tunable and synchronized picosecond-femtosecond double laser system, which is schematically shown in Figure 1. Two independently tunable OPAs are pumped by the output from a picosecond regenerative amplifier operating at 1 kHz repetition rate, 3 mJ pulse energy with 4 ps pulse duration and at 790 nm. By using sum- and difference frequency mixings, we have obtained the continuous tuning of light between 189 and 11200 nm with keeping microjoule pulse energy. Another OPA is excited by the output from a femtosecond regenerative amplifier (1 kHz, 2 mJ, 200 fs, 800 nm) to generate femtosecond pulses over a 300-10000 nm spectral range. A portion of the output from the femtosecond regenerative amplifier is separated and used for harmonic generations. The pulse energy obtained is about 120 μJ for the third harmonic and about 10 μJ for the fourth harmonic, when amplified pulses with 1 mJ pulse energy are used. Two femtosecond mode-locked Ti:sapphire lasers are used to seed the picosecond and femtosecond regenerative amplifiers, respectively. The phase-detection method is adopted to lock the timing of the femtosecond lasers. A typical cross correlation function of pulses from the femtosecond lasers is shown in Figure 2a. The FWHM of the cross-correlation is observed to be 2.5 ps, which corresponds to the timing jitter between pulses from the femtosecond lasers. The two regenerative amplifiers are excited by the output from Q-switched cw Nd:YLF lasers, which are triggered externally by the output from one of the femtosecond laser. Figure 2b shows the cross correlation function of pulses from the regenerative amplifiers. The FWHM of the cross-correlation is found to be about 8 ps, indicating that the regenerative amplifiers are synchronized with the timing jitter of several picoseconds. The femtosecond regenerative amplifier has also been modified to be further excited by a Q-switched pulsed Nd:YAG laser to generate amplified pulses with 10 mJ pulse energy at 10 Hz repetition rate. We have observed time-resolved absorption and Raman spectra of some polyatomic molecules by using this laser system.
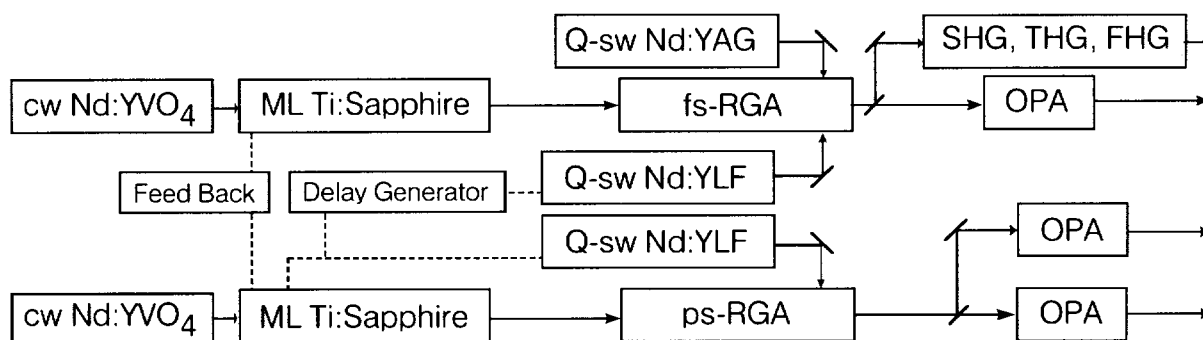
Figure 1. Block diagram of the picosecond-femtosecond double laser system.
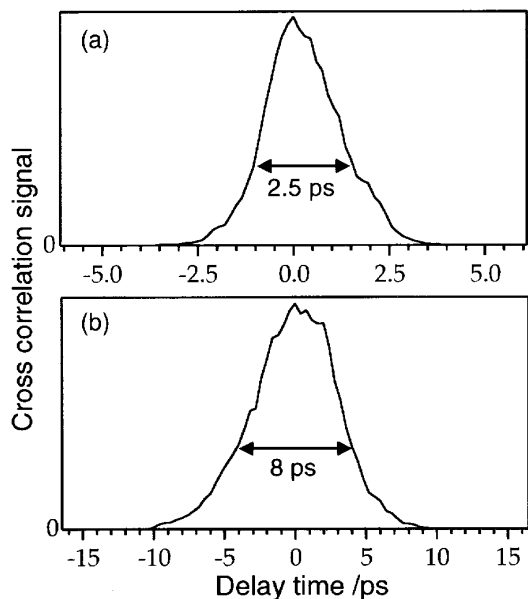
Figure 2. Cross correlation functions observed for pulses from (a) the femtosecond mode-locked lasers and (b) the picosecond and femtosecond regenerative amplifiers.

III-C Spectroscopic and Dynamical Studies on Charge Delocalization and Charge Transfer in Aromatic Molecular Cluster Ions

Charge transfer processes resulting in dynamical charge delocalization such as consecutive proton or electron hopping in molecular clusters and even in pure liquids are highly interesting in relation to the charge transportation in insulating materials. Not only in aromatic molecular liquids but also in pure water itself electric conductivity is very low when they do not contain impurities of ionic atoms or molecules. It is possible to control charge hopping with near infrared photons in such aromatic liquids. Here we investigate the role of impurity or neighboring molecules in changing the electronic properties of benzene cluster cations.

III-C-1 Photodissociation Spectroscopy of Benzene-Acetic acid Mixed Cluster Ions

KOSUGI, Kentaroh; INOKUCHI, Yoshiya; NISHI, Nobuyuki

It is now well known that the charge resonance interactions between the π-electron systems dominate the structures of the benzene cluster ions. On the other hand, the π electrons of the carboxyl group of acetic acid is expected to show strong interaction with the π-electron systems of the aromatic cations. In this study, we measure the photodissociation spectra of benzene-acetic acid mixed cluster ions for investigating the positive charge localization and the structure of the binary complexes.

The experiment is done by using a tandem mass spectrometer coupled with infrared (IR), near IR, and visible lasers. Figure 1(a) displays the photodissociation spectra of $[(C_6H_6)_2(CH_3COOH)_n]^+$ with $n = 1$–4 in the near IR region. All the spectra show very broad bands with a maximum at 920 nm. Since the spectral features well resemble that of benzene dimer cation, we ascribe the bands to the charge resonance bands of benzene dimer ion cores in $[(C_6H_6)_2(CH_3COOH)_n]^+$. In the mixed cluster ions, the positive charge is localized in the benzene dimer site. The photodissociation spectrum in the IR region is thought to be a much better probe of the cluster structure. Figure 1(b) shows the photodissociation spectrum of $[(C_6H_6)_2(CH_3COOH)_1]^+$ in the

IR region. Three bands emerge at 3084, 3585, and 3627 cm^{-1}. According to the spectrum of $[(C_6H_6)_2(CD_3\text{-}COOD)_1]^+$, the band at 3084 cm^{-1} is assigned to the CH stretching vibration of the benzene dimer ion core, and the bands at 3585 and 3627 cm^{-1} are to the OH stretching vibrations of acetic acid. The two OH stretching vibrations imply the existence of two isomers. Possible isomers are *cis*- and *trans*-acetic acid molecules in $[(C_6H_6)_2(CH_3COOH)_1]^+$. In the gas phase, the free OH stretching vibration of a *cis*-acetic acid monomer emerges at 3583 cm^{-1}. Theoretical investigation of the acetic acid monomer by Turi et al. implied that the OH stretching vibration of *trans*-acetic acid has higher frequency than that of the *cis*-acetic acid. According to the facts, we can assign the band at 3585 cm^{-1} to the OH stretching vibration of $[(C_6H_6)_2(cis\text{-}CH_3COOH)_1]^+$, and the band at 3627 cm^{-1} to that of $[(C_6H_6)_2(trans\text{-}CH_3COOH)_1]^+$. In these ions, the acetic acid points the lone pair electrons on the oxygen of the carbonyl group to the benzene dimer ion core, and the OH group of the acetic acid is free from any binding. The benzene dimer ion core makes the *trans*-acetic acid comparatively stable with the *cis*-acetic acid, and the OH vibrations of both *cis*- and *trans*-acetic acid molecules in $[(C_6H_6)_2(CH_3COOH)_1]^+$ are observed in the IR spectrum.
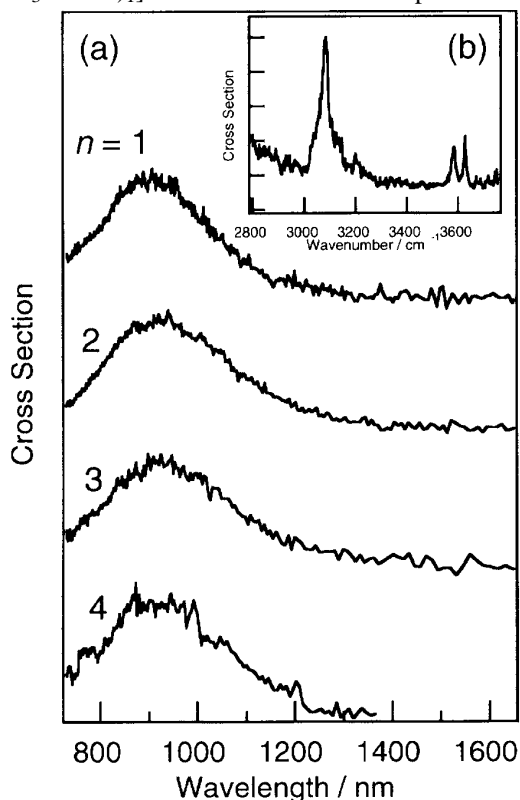
Figure 1. (a) Photodissociation spectra of $[(C_6H_6)_2(CH_3COOH)_n]^+$ with $n = 1$–4 in the near IR region. (b) Photodissociation spectrum of $[(C_6H_6)_2(CH_3COOH)_1]^+$ in the IR region.

III-C-2 Structural Isomers of Benzene-Phenol Mixed Dimer Cation

INOKUCHI, Yoshiya; NISHI, Nobuyuki

The benzene dimer cation with a parallel sandwich structure has a broad and strong absorption band at 920 nm. This band is assigned to the charge resonance (CR) band. The existence of the CR band implies that the positive charge is delocalized in the parallel dimer. On the other hand, the benzene-phenol mixed dimer cation does not show any strong band in the near infrared (IR) region. Therefore, the structure of the mixed dimer cation is thought to be dominated with the hydrogen bonding of the OH group to the π electrons of the benzene. We measure the photodissociation spectra of ordinary and deuterated benzene-phenol mixed dimer cations in the IR region in order to get information on their structures with the help of theoretical calculation.

Figure 1 displays the photodissociation spectra of the benzene-phenol mixed dimer cations. The spectrum at the top is similar to that measured by Mikami *et al.* There are two maxima at 3200 and 3060 cm^{-1}. These bands could be assigned to the OH stretching vibration and CH stretching vibrations of the mixed dimer cation. We also measure the spectrum of the deuterated mixed dimer cation, $[(C_6D_6)(C_6D_5OH)]^+$, showed in the bottom of Figure 1. The spectral feature of the deuterated cation is almost the same as that of the non-deuterated one. Thus, we can confirm that both bands are ascribed to the OH stretching vibrations. Appearance of the two OH stretching vibrations suggests that there are two structural isomers. The frequency of 3060 cm^{-1} is very low as a normal OH stretching frequency, even for a hydrogen-bonded dimer. One possibility is a proton transferred ion complex, $[(C_6H_6\text{-}H^+)\cdots(OC_6H_5)]\longleftrightarrow[(C_6H_6)\cdots(H^+\text{-}OC_6H_5)]$. *Cis*- and *trans*-type orientation of the two aromatic rings must be responsible for the presence of the two peaks in the IR spectra. A theoretical calculation with various basis sets is now going on for checking the validity of the assignment.
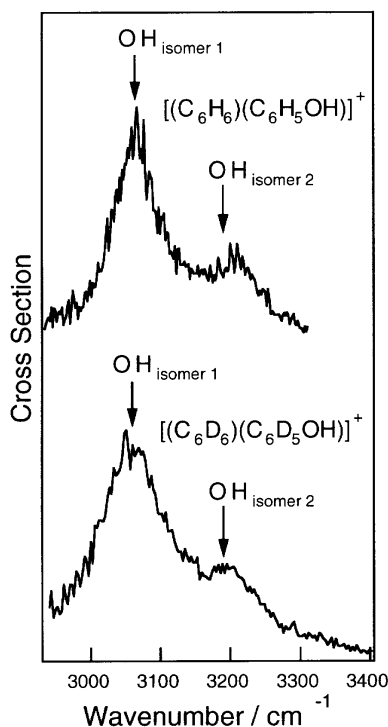
Figure 1. Photodissociation spectra of $[(C_6H_6)(C_6H_5OH)]^+$ (top) and $[(C_6D_6)(C_6D_5OH)]^+$ (bottom) in the IR region.

III-D Spectroscopy and Dynamics of Vibrationally Excited Molecules and Clusters

This research group, which started in April 1997, is planning to study spectroscopy and dynamics of molecules and clusters in higher vibrational state by two-color double resonance spectroscopy. New spectroscopic methods will also be developed to observe the higher vibrational state under collision-free condition.

III-D-1 Overtone Spectroscopy of Jet-Cooled Phenol Studied by Nonresonant Ionization Detected IR Spectroscopy

ISHIUCHI, Shun-ichi[1]; FUJII, Masaaki
(*[1]GUAS*)

Vibrational transitions of jet-cooled phenol have been detected by nonresonant two-photon ionization due to UV laser from 3400 cm^{-1} to 14000 cm^{-1}. The UV frequency dependence of IR-UV double resonance signals is used for discussion on the mechanism of ionization. The spectrum shows a well-resolved structure due to the first to the fourth quantum of OH stretching vibrations, CH overtones and various combination vibrations. The vibrational frequency, anharmonisity and the dissociation energy of the OH stretching mode has been measured. The bandwidth of the OH overtone is found to decrease with increase in the vibrational quantum number.

III-C-2 Structure of 1-Naphthol-Water Clusters Studied by IR Dip Spectroscopy and Ab Initio Molecular Orbital Calculation

YOSHINO, Ruriko[1]; HASHIMOTO, Kenro[2]; OMI, Takuichiro[1]; ISHIUCHI, Shun-ichi[3]; FUJII, Masaaki
(*[1]Waseda Univ.; [2]Tokyo Metropolitan Univ.; [3]GUAS*)

IR spectrum of *cis*-1-naphthol, *trans*-1-naphthol, and 1-naphthol·$(H_2O)_n$ ($n = 1–3$) clusters has been measured by the IR dip spectroscopy in a supersonic jet. The spectra show clear vibrational structures of the monomers and the clusters in the energy region from 3000 cm^{-1} to 3800 cm^{-1}. Observed vibrational transitions are assigned to the OH stretching vibrations of 1-naphthol and waters in the clusters. The size dependence of the IR bands and the cluster geometries are analyzed by using the ab initio MO method at MP2/6-31G level. From the comparison between the observed and calculated IR spectra, we have concluded that the 1-naphthol acts as the proton donor and a cyclic hydrogen-bond network is formed in the $n = 2$ and 3 clusters.

III-E Femtosecond Time-Resolved Photoelectron Imaging

Photodissociation dynamics has been studied extensively by measuring quantum state and scattering distributions of products. However, the most unambiguous experimental elucidation of reaction mechanism is by real-time observation of the reaction. Photoelectron spectroscopy is useful for this purpose, since it projects the wavepacket dynamics in the excited state to an accurately-known cation potential. Other advantages of photo-electron spectroscopy are (1) capability of detecting both singlet and triplet states, enabling direct observation of intersystem crossing and internal conversion processes, (2) high sensitivity due to efficient collection of electrons by electromagnetic fields, and (3) applicability of ultrafast laser with fixed wavelength. The analysis of photoelectron scattering distribution has been performed most often by the time-of-flight (TOF) method. However, a standard TOF method has a poor collection efficiency of electrons. The magnetic bottle spectrometer significantly improved the efficiency, but angular resolution is sacrificed. Photoelecton imaging (PEI) achieves the highest collection efficiency of electrons while providing routine measurements of speed and angular distributions. This work presents PEI coupled with femtosecond pump-probe technique, for the first time.

III-E-1 Femtosecond Time-Resolved Photo-electron Imaging on Ultrafast Electronic Dephasing in an Isolated Molecule

SUZUKI, Toshinori; WANG, Li; KOHGUCHI, Hiroshi

The femtosecond time-resolved photoelectron imaging is reported for the first time. The method was applied to ultrafast dephasing in an intermediate case molecule Pyrazine. Figure 1 shows the snapshot of photoelectron scattering distribution measured as a function of pump-probe time delay. The decay of the optically-prepared S_1 character (the outer ring) and the build-up of dark triplet character (the inner ring) are clearly seen. The result also suggests the possibility that intersystem crossing is mediated by $T_2(\pi,\pi^*)$ state. This work is the first direct observation of the dynamics in the triplet manifold of this benchmark system.
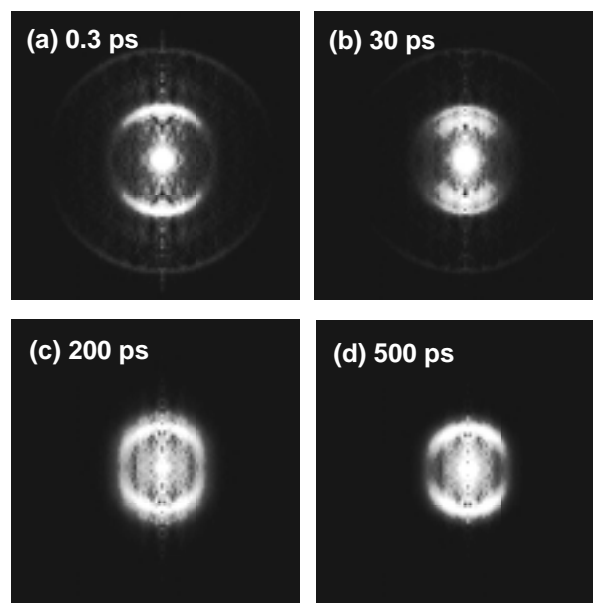
Figure 1. Inverse Abel transforms (512×512 pixels) of photoelectron images of [1+2'] REMPI of Pyrazine via the $S_1[^1B_{3u}(n,\pi^*)] 0^0$ level at the time delays of (a) 0.3, (b) 30, (c) 200, and (d) 500 ps. The original images were integrated for 36 000 laser shots.

III-F Dynamical Stereochemistry

Stereodynamics in molecular photodissociation is investigated experimentally and theoretically. Efforts are made to determine multipole moments (density matrix) of a photofragment completely and interpret them quantum-mechanically.

III-F-1 Vector Correlation in Molecular Photo-dissociation

MO, Yuxiang; SUZUKI, Toshinori

The quantum mechanical expression for the angle-dependent photofragment multiple moments is rigorously derived with only the dipole approximation. The angular momentum coupling between the two fragments is taken into account for the first time. The result is also compared with the *formal expansion method* assuming fixed **μ-v-J** vector correlation for all scattering angles [Y. Mo and T. Suzuki, *J. Chem. Phys.* **108**, 6780 (1998)]. The condition that reduces the rigorous formula to the approximate formula is examined.

III-G Photochemistry on Well-Defined Surfaces

Upon the irradiation of light in the wavelength range from visible to ultraviolet, a number of adsorbed molecules on metal surfaces reveal variety of photochemical processes, including photo-stimulated desorption, rearrangement of adsorbed states, photodissociation, and photo-initiated reactions with coadsorbates. A central and fundamental question in the surface photochemistry is to clarify how adsorbate-substrate systems are excited by photon irradiation. In addition, since photo-initiated reactions can be induced without any thermal activation of reactants, they may provide good opportunities for studying a new class of surface reactions which may not be induced thermally. We have studied photochemistry of various adsorption systems on well-defined metal and semiconductor surfaces mainly by temperature-programmed desorption (TPD), x-ray photoelectron spectroscopy (XPS), work function measurements, near edge x-ray absorption fine structure (NEXAFS) and angular-resolved time-of-flight (TOF) spectroscopy of photodesorbed species associated with pulsed laser irradiation. We have shown that methane weakly adsorbed on Pt(111) and Pd(111) is dissociated or desorbed by irradiation of 6.4-eV photons, which is far below the excitation energy for the first optically allowed transition of methane in the gas phase. This work has been extended to Cu(111), where photo-induced C-C coupling takes place. In addition, more thorough investigations have been done on the photodesorption of rare gas atoms from clean and modified Si(100) surfaces.

III-G-1 Photo-stimulated Desorption of Rare Gas Atoms Induced by UV-NIR Photons at a Semiconductor Surface

WATANABE, Kazuya; MATSUMOTO, Yoshiyasu

[*Surf. Sci. Lett.* submitted]

Desorption induced by electronic transitions (DIET) of rare gases provides a good opportunity for understanding fundamental questions in electron- and photon-induced surface processes because no internal nuclear motions are involved compared with other DIET of polyatomic adsorbates. The DIET of rare gas atoms has been observed in the past by using electrons or photons whose energy exceeds 7 eV, since it requires high energy to ionize or excite valence- and core-electrons of rare gas atoms. However, we show that heavy rare gas atoms (Kr and Xe) are desorbed from clean and modified Si(100) surfaces by irradiating photons with energy as low as 1.16 eV.

Rare gas atoms are adsorbed on the surfaces at 50 K. UV and visible photons are irradiated onto the surfaces. Post-irradiation TPD is observed as a function of irradiated photon numbers. The area of TPD peaks decreases with increase of the number of photons, indicating the coverage of Xe is reduced by the photon irradiation. On the clean Si(100) surface, the kinetic energy distributions of the rare gas atoms are well represented by the Maxwell-Boltzmann distribution, but the obtained temperature is quite higher than that expected by surface heating with employed laser fluence. Furthermore, they do not depend on the excitation photon energy from 1.16 eV to 6.43 eV nor on the laser fluence. Thus, these features cannot be explained by conventional laser-induced thermal desorption. The most plausible mechanism for the desorption is that hot surface phonons created by recombination of photo-generated electron-hole pairs at a semiconductor surface directly couple to the desorption channel before they decay into bulk phonons.

III-G-2 Photochemistry of Methane on Cu(111)

WATANABE, Kazuo; MATSUMOTO, Yoshiyasu

[*Surf. Sci.* in press]

Conversion of methane into useful chemical reagents has been extensively studied for several decades owing to the increasing industrial and environmental importance. However, methane is the most stable hydrocarbon and the previous efforts to break the methane C-H bond *thermally* have not necessary been successful regarding the efficiency and costs even with sophisticated catalysts.

In this work photochemistry of methane physisorbed on Cu(111) at 35 K have been investigated by temperature-programmed desorption (TPD). Methane is photodissociated into hydrogen, methylene, and methyl by 6.4-eV photon irradiation as in the case of Pt(111) and Pd(111). However, there are unique features on Cu(111). Post-irradiation TPD showed new desorption peaks of ethylene at 115 K and 380 K, in addition to the 430 K peak reported before. They are attributed to molecular desorption of ethylene formed by methane photodissociation at 35 K, associative recombination of two methylene groups, and concerted reactions of four methyl groups, respectively. The photoreaction cross section is estimated 2.0×10^{-20} cm^2. Thus, photochemical C-C coupling in the photochemistry of methane is observed for the first time.

III-G-3 Coadsorption Effect of Cs on Photochemistry of Methane on Pt(111)

ANAZAWA, Toshihisa; WATANABE, Kazuo; MATSUMOTO, Yoshiyasu

We have reported that methane on Pt(111) is dissociated by irradiating uv photons.[1] The excitation is understood as a transition from the ground state localized at methane to the excited state of the methane-substrate atoms complex where the excited Rydberg-like state of methane significantly mixed with the substrate empty states. Another way to understand the excitation mechanism is in the following. When the complete charge transfer to the substrate is assumed in the excited state of methane, the image force stabilizes the excited state by 1.9 eV. The ionization potential of physisorbed methane should then be reduced by 1.9 eV + the work function of the metal. Taking a work

function of 5.6 eV and the gas phase ionization potential of 12.6 eV, the excitation energy for the complete charge transferred state is calculated to be 5.1 eV, which is accessible with a 6.4-eV photon. When Cs is adsorbed, the work function is significantly reduced. By using this feature, we measured how the photochemical cross section is affected by the coadsorption of Cs to examine further the excitation mechanism. The measurements show that the cross section is significantly reduced by the Cs coadsorption, in agreement with the expectation of the complete charge transfer model.

Reference
1) Y. Matsumoto, Y. A. Gruzdkov, K. Watanabe and K. Sawabe, *J. Chem. Phys.* **105**, 4775 (1996).

III-H Multiphoton Photoelectron Spectroscopy of Electronic States at Metal Surfaces

A central and fundamental question in surface photochemistry is to clarify how adsorbate-substrate systems are excited with photon irradiation. Thus, direct information on the excited states at surfaces is needed. One of the best methods, and most relevant to surface photochemical measurements, is multiphoton photoelectron spectroscopy. We have extended this method by using two-color (visible and VUV) beams for pump-and-probe experiments. In this year, the method is applied to surface states of clean and Xe-covered Pt(111) surfaces.

III-H-1 Visible and VUV Two-Photon Photo-electron Spectroscopy of the Surface State of a Clean Pt(111) Surface

KINOSHITA, Ikuo[1]; WATANABE, Kazuya; INO, Daisuke[2]; MATSUMOTO, Yoshiyasu
(*[1]Yokohama City Univ.; [2]GUAS*)

The sp-derived surface state of a clean Pt(111) surface has been experimentally confirmed by visible two-photon photoelectron spectroscopy.[1] We have extended this measurement by using visible and VUV photons. This method allows us to detect empty states near the Fermi level. The VUV photons are generated by tripling the frequency-doubled Ti:sapphire output in a Xe cell. Photoelectons are detected and analyzed by a time-of-flight electron energy analyzer. The surface state is located at 0.2 eV below the Fermi level when detected along the surface normal. Since this state has a free-electron like parabolic dispersion curve, the state is expected to be unoccupied at large parallel momenta. In fact, we found that the photoelectron peak originating in the empty surface state appears at large detection angles from the surface normal. This gives a more complete picture of the dispersion curve of the surface state.

Reference
1) I. Kinoshita, T. Anazawa and Y. Matsumoto, *Chem. Phys. Lett.* **229**, 445 (1996).

III-I Ultrafast Reaction Dynamics of Photochromism and Related Phenomena

Photochromic reactions of some organic molecules are of considerable interest because of their wide applications including optical information processing, data storage, and nonlinear optics. The photochromism defined as a reversible transformation in chemical species between two forms is based on simple photochemical reactions such as bond cleavage, pericyclic, proton transfer, and isomerization reactions. As a result of different molecular structures between these two forms, the two isomers differ from one another in various properties such as absorption spectra, dipole moments, refractive indices, and so on. To understand the primary processes and functional properties of photochromic systems, we have examined several photochromic compounds by femtosecond and picosecond laser spectroscopic techniques.

III-I-1 Time-Resolved Study on Unconventional Fluorescence of an Azobenzene Liquid Crystal and Its Phase Transition

AZUMA, Jun[1]; TAMAI, Naoto[1,2]; SHISHIDO, Atsushi[3]; IKEDA, Tomiki[3]
(*[1]Kwansei Gakuin Univ.; [2]IMS; [3]Tokyo Inst. Tech.*)

As far as the luminescence of azobenzene derivatives is concerned, it is well known that azobenzene do not show appreciable emission because of the trans-cis isomerization and the $n\pi^*$ character of the first-excited singlet state. Fluorescence properties of azobenzene liquid crystal, 4,4'-dioctyloxy-azobenzene (8AB8), were examined by steady-state and picosecond single-photon timing spectroscopy. It was found that the fluorescence from azobenzene aggregate with a peak at ~ 630 nm was observed in the solid phase in addition to the very weak S_2 fluorescence of azobenzene monomer centered at 420 nm. The structure of aggregate was estimated to be J-like structure. The fluorescence lifetimes of both J-aggregate and monomer S_2 state were estimated to be approximately 150 ps and shorter than 2 ps. The fluorescence lifetime of J-aggregate and relative fluorescence intensity of aggregate/monomer were found to be strongly dependent on temperature and liquid crystalline phases. Microscopic aggregate structure of 8AB8 in various liquid crystalline phases was discussed on the basis of these results.

III-I-2 Solvation Dynamics of Excited p-Methoxy-p'-cyanodiphenylacetylene in n-Butanol: Simultaneous Analysis of Time-Resolved Fluorescence Anisotropy and Stokes Shift

TAMAI, Naoto[1,2]; NOMOTO, Takeo[3], TANAKA, Fumio[4]; MATAGA, Noboru[5]
(*[1]Kwansei Gakuin Univ.; [2]IMS; [3]Mie Univ.; [4]Mie Pref. College of Nursing; [5]Inst. Laser Tech.*)

Solvation dynamics of p-methoxy-p'-cyano-diphenylacetylene in n-butanol was investigated by observing time-resolved fluorescence anisotropy and dynamic Stokes shift in picosecond time domain. Fluorescence spectra of p-methoxy-p'-cyanodiphenyl-acetylene exhibited a large Stokes shift, depending on the solvent polarity. The observed time-resolved anisotropy and Stokes shift were simultaneously analyzed with the theory based on the continuum model, in which dielectric friction in polar solvent was introduced through rotational motion of solute molecules with non-Markov process according to the framework of Nee and Zwanzig. The both experimental decays satisfactory fit with the theory. The dipole moments in the excited state and the ground state were estimated to be ~ 14 Debye and negligibly small.

III-I-3 A Combined Experimental and Theoretical Study on the Photochromism of Aromatic Anils

MITRA, Sivaprasad[1]; TAMAI, Naoto[1,2]
(*[1]Kwansei Gakuin Univ.; [2]IMS*)

Dynamics of photochromism have been studied in anil compounds using femtosecond transient absorption and picosecond fluorescence spectroscopies. The experimental observations were compared with the theoretical results obtained from AM1-SCF calculations. Excited-state intramolecular proton transfer (ESIPT) and photochromic reactions were found to occur from the S_1 state whereas normal fluorescence appears from the second excited singlet state. The photochromic processes are seen to be very fast which occur within few hundred of femtoseconds. The lifetime of the S_2 state was observed to be relatively long. This slower decay from higher excited singlet state was explained on the basis of the mixed nature of electronic transition comprising this state and relatively weak $S_2 \leftarrow S_1$ internal conversion. Theoretical results predict the ESIPT state to be zwitterionic in character, however, the final product may be a mixture of zwitter-ionic and nonionic in nature.

III-I-4 Photochromism in 2-(2',4'-Dinitrobenzyl)-pyridine Studied by Ultrafast Laser Spectroscopy

MITRA, Sivaprasad[1]; ITO, Hirotsugu[1]; TAMAI, Naoto[1,2]
(*[1]Kwansei Gakuin Univ.; [2]IMS*)

Ultrafast transient behavior of photochromic 2-(2',4'-dinitrobenzyl)pyridine have been studied using femtosecond transient absorption spectroscopy. Three

different transient signals could be found in the experiment at different time delays. The dynamics of the transient behavior in the short time scale reveal that very fast relaxation (within ~ 400 ± 100 fs) from the initial excited state leads to the formation of a relatively stable intermediate which is the precursor of excited state proton transfer. This intermediate decays to the ground state of proton transferred aci-nitro structure in nanosecond time scale. Solvent hydrogen bonding in ethanol plays an important role in the deactivation of the excited state giving different photophysical behavior.

III-J Photophysics and Photochemistry in Interface Layers and Mesoscopic Systems

Photochemical and photophysical processes in thin films, liquid/electrode interface layers, and some confined systems are considerable interest because of their characteristic properties different from those in the bulk. For analyzing the dynamics in these systems, we have applied various ultrafast spectroscopic techniques such as femtosecond transient grating spectroscopy, picosecond single-photon timing spectroscopy, and scanning probe microscopy (SPM). The development of time-resolved scanning near-field optical microscopy (SNOM) and STM are indispensable for these studies. The mesoscopic structures and dynamics of molecular aggregates on solid surfaces have been examined by time-resolved SPM. The photoelectrochemistry is an another important subject to analyze the role of interface layers. The characteristic properties of carrier and electron transfer dynamics in liquid/electrode interface layers have been also examined by femtosecond laser spectroscopy.

III-J-1 Time-Resolved and Near-Field Scanning Optical Microscopy Study on Porphyrin J-Aggregate

MIURA, Atsushi[1]; MATSUMURA, Kazuo[1]; SU, Xingguang[1]; TAMAI, Naoto[1,2]
(*[1]Kwansei Gakuin Univ.; [2]IMS*)

[*Acta Phys. Pol.* **94**, 835 (1998)]

Water-soluble porphyrin, 5,10,15,20-tetraphenyl-21H,23H-porphinetetrasulfonic acid (TPPS), forms J-aggregate in aqueous solution depending on experimental conditions such as pH, dye concentration, and/or ionic strength. The steady-state fluorescence and picosecond single-photon timing spectroscopy were applied for protonated monomer and J-aggregate in aqueous solution and in thin films to reveal the dynamics in the S_2 and S_1 states. The S_2 fluorescence spectra from the protonated monomer and J-aggregate were observed in addition to the normal S_1 fluorescence. The lifetime of the S_2 state was estimated to be shorter than a few ps for J-aggregate. The mesoscopic structures of J-aggregate in thin film with and without polymer on the glass surface were examined by scanning near-field optical microscopy (SNOM). With the surface topography and SNOM transmission images, TPPS J-aggregate was found to form a long and narrow tube-like structure which has a few μm length, 0.2~0.5 μm width, and 5~30 nm height. An unidirectional orientation of the structure was also found, which may be originated from the spin-coating process.

III-J-2 Excitation Energy Transfer in Langmuir-Blodgett Films of 5-(4-N-Octadecylpyridyl)-10,15,20-tri-p-tolylporphyrin on Gold-Evaporated Glass Substrates Studied by Time-resolved Fluorescence Spectroscopy

ZHANG, Zhijun[1]; VERMA, Atul[1]; TAMAI, Naoto[1,2]; NAKASHIMA, Kenichi[3]; YONEYAMA, Michio[4]; IRIYAMA, Keiji[5]; OZAKI, Yukihiro[1]
(*[1]Kwansei Gakuin Univ.; [2]IMS; [3]Saga Univ.; [4]Mitsubishi Chem. Co.; [5]Jikei Univ.*)

[*Thin Solid Films* **333**, 1 (1998)]

The fluorescence decays in mono- and multilayer Langmuir-Blodgett (LB) films of 3-(4-N-octadecyl-pyridil)-10,15,20-tri-p-tolylporphyrin (porphyrin338a) deposited on gold evaporated glass substrates were measured to explore various cannels for excitation energy transfer processes. The decays in the 1-layer LB films of porphyrin 338a separated from gold surface by LB film of arachidic acid were also measured as a function of the thickness of spacer, *i.e.* the thickness of the LB films of arachidic acid. Consistent with our previous steady-state fluorescence study, the expectation values of the lifetime obtained by fitting the decay curves indicate that at the short separation distance, the energy transfer from the porphyrin molecules to the gold surface overshadows other processes, including intra- and interlayer energy transfers. The deviation of energy transfer rate from Chance *et al.* (CPS) prediction of inverse distance cubed in our case may be interpreted by assuming the presence of additional excitation energy decay pathways in the LB films of porphyrin 338a on the gold evaporated glass substrates.

III-J-3 Carrier Dynamics on Titanium Dioxide Single Crystals by Femtosecond Transient Grating Spectroscopy

YANG, Xiujuan[1]; TAMAI, Naoto[1,2]; NAKATO, Yoshihiro[3]
(*[1]Kwansei Gakuin Univ.; [2]IMS; [3]Osaka Univ.*)

The photogenerated carrier dynamics in bare titanium dioxide (TiO_2) single crystals with (100), (110), and (001) faces was examined by femtosecond transient grating spectroscopy. The dynamics of transient grating signal at low excitation intensity was

found to be very similar to that of the luminescence observed at ~ 430 nm, suggesting that the same species were probed by both time-resolved spectroscopies existing in the surface layer of TiO_2 single crystals. The decay curves of transient grating were strongly dependent on the excitation intensity but independent on the types of crystal faces. The rate of the formation of Γ-state or electron trapping in TiO_2 single crystal was found to be faster than 50 fs. The subsequent intensity-dependent relaxation was analyzed in terms of electron-hole recombination kinetics, and the recombination rate constants in single crystals were compared with that of TiO_2 nanoparticles.